

Nanostructured Lipid Carriers for Enhanced Oral Delivery of Antidiabetic Phytochemicals

Mohammad Intakhab Alam¹, Abduganieva Arofat Yormakhamatovna², Jeevanandham Somasundaram³, Suparna Pal Deb⁴, Madhavi Latha Samala⁵, Pulatova Kristina Samvelovna⁶, Srinivas Murthy B R^{7*}

¹Mohammad Intakhab Alam, Assistant Professor, Department of Pharmaceutics, College of Pharmacy, Jazan University, Jazan, KSA

²Abduganieva Arofat Yormakhamatovna, Senior Lecturer, Department of Epidemiology and Infectious Diseases, Fergana Medical Institute of Public Health, Fergana, Uzbekistan

³Dr. Jeevanandham Somasundaram, Director, Professor of Pharmaceutics, Sri Shanmugha College of Pharmacy (Affiliated to The Tamil Nadu Dr. M.G.R. Medical University, Chennai), Pullipalayam, Morur (Po), Sankari (Tk), Salem District, Tamil Nadu – 637 304, India

⁴Suparna Pal Deb, Assistant Professor, JIS College of Engineering, Kalyani, Nadia, West Bengal – 741235, India

⁵Madhavi Latha Samala, Associate Professor, Aditya College of Pharmacy, Aditya Nagar, ADB Road, Surampalem, Kakinada District, Andhra Pradesh – 533437, India

⁶Pulatova Kristina Samvelovna, Assistant of the department of internal diseases and cardiology no2, Samarkand state medical University, Samarkand, Uzbekistan; Orcid: 0000-0001-6637-3078; Email: davitty_girl@mail.ru.

^{7*}Srinivas Murthy B R, Assistant Professor, College of Pharmaceutical Sciences, Dayananda Sagar University, Harohalli, Bengaluru – 562112, Karnataka, India. Email: seenu46@gmail.com. Corresponding Author.

ABSTRACT

Antidiabetic phytochemicals including berberine, quercetin, and curcumin demonstrate potent pharmacological activities but are hampered by poor oral bioavailability attributable to low aqueous solubility, extensive first-pass metabolism, P-glycoprotein-mediated efflux, and limited intestinal permeability. Nanostructured lipid carriers (NLCs), second-generation lipid-based nanoparticles composed of a blend of solid and liquid lipids, represent a promising strategy to overcome these biopharmaceutical barriers. The present study describes the systematic formulation, optimisation, and in vitro evaluation of berberine-loaded NLCs (NLC-F1 to NLC-F8) prepared by hot melt homogenisation-ultrasonication. Formulations were characterised for particle size, polydispersity index (PDI), zeta potential, encapsulation efficiency (EE%), and drug loading. The optimised formulation NLC-F3 exhibited a particle size of 148.2 ± 3.6 nm, PDI of 0.198 ± 0.009 , zeta potential of -38.2 ± 1.4 mV, and EE of $91.8 \pm 1.6\%$. In vitro drug release studies demonstrated 88.6% cumulative release at 24 h at pH 6.8. Caco-2 permeability studies confirmed a 3.02-fold improvement in apparent permeability coefficient compared to pure berberine. NLC-F3 also exhibited superior α -glucosidase inhibitory activity ($IC_{50} = 38.6$ μ g/mL) relative to free berberine ($IC_{50} = 68.4$ μ g/mL; $p < 0.001$). These findings confirm that NLC encapsulation significantly enhances oral bioavailability and antidiabetic efficacy of berberine, warranting further preclinical and clinical investigation.

Keywords: Nanostructured lipid carriers; berberine; antidiabetic; oral bioavailability; phytochemicals; Caco-2 permeation; α -glucosidase inhibition; hot melt homogenisation; encapsulation efficiency; controlled release

How to cite this article: Alam MI, Yormakhamatovna AA, Somasundaram J, Deb SP, Samala ML, Samvelovna PK, B R SM. Nanostructured Lipid Carriers for Enhanced Oral Delivery of Antidiabetic Phytochemicals. *Int J Drug Deliv Technol.* 2026;16(17s): 568-580. DOI: 10.25258/ijddt.16.17s.67

Source of support: Nil.

Conflict of interest: None

1. Introduction

Type 2 diabetes mellitus (T2DM) is a chronic metabolic disorder of global pandemic proportions, affecting approximately 537 million adults in 2021 with projections reaching 783 million by 2045.¹ The pathophysiology of T2DM is multifactorial, encompassing peripheral insulin

resistance, progressive pancreatic β -cell dysfunction, dysregulated hepatic glucose output, and chronic low-grade inflammation.² Despite the availability of numerous synthetic antidiabetic agents, including metformin, sulfonylureas, DPP-4 inhibitors, and GLP-1 receptor agonists, persistent challenges related to adverse effects,

therapeutic failure over time, and high cost have intensified interest in phytochemical-based therapeutic alternatives.³ Antidiabetic phytochemicals — including berberine, quercetin, curcumin, resveratrol, and piperine — have demonstrated potent multi-target antidiabetic activities, including inhibition of α -amylase and α -glucosidase, stimulation of insulin secretion and signalling, activation of AMP-activated protein kinase (AMPK), reduction of hepatic gluconeogenesis, and suppression of inflammatory pathways.⁴ Berberine, an isoquinoline alkaloid isolated from *Berberis aristata* and related plants, has been extensively studied and shown to reduce fasting blood glucose and HbA1c levels with efficacy comparable to metformin in clinical trials.⁵ However, berberine and most antidiabetic phytochemicals suffer from critically poor oral bioavailability attributable to several overlapping barriers: low aqueous solubility (BCS Class IV), extensive intestinal and hepatic first-pass metabolism, active efflux by P-glycoprotein (P-gp) at intestinal epithelium, instability in gastrointestinal fluids, and limited transcellular permeability.⁶

Nanotechnology-based drug delivery systems have emerged as powerful tools to overcome these biopharmaceutical barriers.⁷ Among lipid-based nanocarriers, nanostructured lipid carriers (NLCs) represent the second generation of solid lipid nanoparticles (SLNs), developed to overcome the limitations of SLNs including low drug loading capacity, drug expulsion during storage due to lipid crystallisation, and poor incorporation of hydrophilic drugs.⁸ NLCs are composed of a blend of solid lipid and liquid lipid (oil), forming an imperfect crystalline matrix that provides greater structural disorder, higher drug loading capacity, reduced drug expulsion, and improved physical stability compared to SLNs.⁹ The lipid matrix of NLCs further facilitates lymphatic uptake, bypassing hepatic first-pass metabolism, and the presence of lipids stimulates bile secretion and enhances solubilisation of poorly water-soluble drugs in the gastrointestinal lumen.¹⁰

Several studies have reported NLC formulations for individual phytochemicals such as curcumin¹¹ and quercetin¹², demonstrating marked improvements in oral bioavailability. However, systematic comparative studies evaluating the influence of formulation variables particularly solid-to-liquid lipid ratio, surfactant type and concentration, and co-surfactant selection on the physicochemical properties and in vitro antidiabetic performance of berberine-loaded NLCs remain limited. The present study addresses this gap by developing eight NLC formulations using a rational formulation design approach

and conducting comprehensive physicochemical, release, permeation, and in vitro antidiabetic characterisation, with the objective of identifying an optimised formulation for potential oral antidiabetic application.

2. Materials

Berberine hydrochloride (purity $\geq 98\%$) was procured from Sigma-Aldrich (St. Louis, MO, USA) and used as the model antidiabetic phytochemical throughout the study. Compritol 888 ATO (glyceryl behenate) and Precirol ATO 5 (glyceryl palmitostearate) were gifted by Gattefossé (Saint-Priest, France) and served as solid lipid components. Capryol 90 (propylene glycol monocaprylate) and Labrafil M 1944 CS (linoleoyl macrogol-6 glycerides) were also obtained from Gattefossé as liquid lipid (oil) phase components. Tween 80 (polysorbate 80) and Span 80 (sorbitan monooleate) were purchased from Sigma-Aldrich. Solutol HS 15 (polyoxyl 15 hydroxystearate) was gifted by BASF (Ludwigshafen, Germany). Transcutol HP (diethylene glycol monoethyl ether, used as co-solvent) was supplied by Gattefossé. Porcine pancreatic α -amylase (Type VI-B), α -glucosidase (from *Saccharomyces cerevisiae*), p-nitrophenyl- α -D-glucopyranoside (pNPG), bovine serum albumin (BSA), DPPH (1,1-diphenyl-2-picrylhydrazyl), and acarbose (pharmaceutical standard) were obtained from Sigma-Aldrich. Caco-2 human colon adenocarcinoma cells and L6 rat skeletal muscle cells were procured from the National Centre for Cell Science (NCCS), Pune, India. DMEM, EMEM, FBS, penicillin-streptomycin, and trypsin-EDTA were purchased from Gibco Life Technologies (Carlsbad, CA, USA). The 2-NBDG fluorescent glucose analogue assay kit was obtained from Cayman Chemical (Ann Arbor, MI, USA). Dialysis membranes (MWCO 12,000–14,000 Da) were procured from HiMedia Laboratories (Mumbai, India). All other chemicals and solvents were of analytical or HPLC grade from Merck (Darmstadt, Germany) or HiMedia Laboratories. Ultrapure water (resistivity ≥ 18.2 M Ω ·cm) from a Milli-Q system (Millipore, USA) was used throughout all experiments.

3. Methods

3.1 Solubility and Compatibility Screening of Lipid Excipients

Solubility of berberine hydrochloride in various solid lipids (Compritol 888 ATO, Precirol ATO 5) and liquid lipids (Capryol 90, Labrafil M 1944 CS) was determined by the saturation solubility method. Excess berberine (50 mg) was added to 1 g of each molten lipid (at 5°C above the respective melting point) in sealed glass vials, vortexed for 5 min, and then equilibrated at the melting temperature for 48 h with periodic agitation. Mixtures were centrifuged

Nanostructured Lipid Carriers for Enhanced Oral Delivery of Antidiabetic Phytochemicals

(5000 rpm, 15 min), and the saturated lipid supernatant was dissolved in methanol. Berberine concentration was quantified by HPLC. Lipids showing the highest drug solubility were selected as components of the NLC matrix.¹¹⁻¹⁴ Lipid-drug compatibility was further assessed by differential scanning calorimetry (DSC) binary mixture studies.

3.2 Formulation Design of Nanostructured Lipid Carriers

Eight NLC formulations (NLC-F1 to NLC-F8) were designed by systematically varying four critical formulation variables: solid lipid type (Compritol 888 ATO or Precirol ATO 5), solid-to-liquid lipid ratio, surfactant concentration (Tween 80: 1.0% or 1.5% w/v), and co-surfactant type (Span 80 or Solutol HS 15). The total lipid concentration was fixed at 5% w/v and berberine concentration at 0.5% w/v across all formulations. The detailed formulation design matrix is presented in Table 1.

Table 1. Formulation Design Matrix for Berberine-Loaded NLC Formulations (NLC-F1 to NLC-F8)

F. Code	Solid Lipid	Liquid Lipid	S:L Lipid Ratio	Berberine (%w/v)	Tween 80 (% w/v)	Co-surfactant	Homogenization Cycles
NLC-F1	Compritol 888 ATO	Capryol 90	8:2	0.5	1.0	Span 80 (0.5%)	3
NLC-F2	Compritol 888 ATO	Capryol 90	8:2	0.5	1.5	Span 80 (0.5%)	3
NLC-F3	Compritol 888 ATO	Capryol 90	7:3	0.5	1.5	Solutol HS 15 (0.5%)	5
NLC-F4	Compritol 888 ATO	Labrafil M 1944 CS	7:3	0.5	1.5	Solutol HS 15 (0.5%)	5
NLC-F5	Precirol ATO 5	Capryol 90	8:2	0.5	1.0	Span 80 (0.5%)	3

NLC-F6	Precirol ATO 5	Capryol 90	7:3	0.5	1.5	Span 80 (0.5%)	5
NLC-F7	Precirol ATO 5	Labrafil M 1944 CS	7:3	0.5	1.5	Solutol HS 15 (0.5%)	5
NLC-F8	Precirol ATO 5	Labrafil M 1944 CS	8:2	0.5	1.0	Span 80 (0.5%)	3

3.3 Preparation of NLC Formulations by Hot Melt Homogenisation-Ultrasonication

NLC formulations were prepared by the hot melt homogenisation-ultrasonication method.¹⁵ Briefly, the solid lipid component was melted at 10°C above its melting point in a water bath. The required quantity of liquid lipid and berberine hydrochloride (pre-dissolved in a minimal volume of Transcutol HP) were added to the molten solid lipid and mixed thoroughly at 70°C under continuous magnetic stirring (500 rpm, 15 min) to form a homogeneous lipid melt containing the drug. This constituted the lipid phase. Separately, the aqueous phase was prepared by dissolving the surfactant (Tween 80) and co-surfactant (Span 80 or Solutol HS 15) in ultrapure water and heating to the same temperature (70°C). The aqueous phase was added dropwise to the lipid phase under high-shear homogenisation using an Ultra-Turrax T-25 homogeniser (IKA, Germany) at 12,000 rpm for 5 min to produce a hot pre-emulsion.¹⁶ The hot pre-emulsion was then subjected to probe ultrasonication (Sonics Vibra-Cell VC-505, 40% amplitude, pulsed mode 5 s on/3 s off, ice-water bath) for 3 or 5 cycles (3 min per cycle) as specified in Table 1, to produce a nanoemulsion. The nanoemulsion was immediately cooled to room temperature under gentle stirring (300 rpm) to induce crystallisation and form solid NLCs. The resulting NLC dispersions were stored at 4°C in sealed amber vials for characterisation. Blank NLC formulations (without berberine) were prepared identically for FTIR and DSC comparison studies.

3.4 Particle Size, PDI, and Zeta Potential Analysis

Hydrodynamic particle size, polydispersity index (PDI), and zeta potential of all NLC formulations were determined using a Malvern Zetasizer Nano ZS instrument (Malvern

Nanostructured Lipid Carriers for Enhanced Oral Delivery of Antidiabetic Phytochemicals

Instruments, UK) with a 633 nm He-Ne laser at a backscattering angle of 173° (NIBS technology). NLC dispersions were diluted 1:100 with ultrapure water (to minimise multiple scattering) and equilibrated at 25°C for 2 min before measurement. DLS was performed in triplicate (12 sub-runs per measurement). Results are expressed as z-average diameter (intensity-weighted mean hydrodynamic diameter) ± SD. Zeta potential was measured using the same instrument in electrophoretic light scattering (ELS) mode with DTS1070 folded capillary zeta cells. All measurements were performed at 25°C. Absolute zeta potential values > 30 mV were considered indicative of excellent colloidal stability.^{17,18}

3.5 Encapsulation Efficiency (EE%) and Drug Loading (DL%) Determination

Encapsulation efficiency was determined by indirect method. Freshly prepared NLC dispersions were ultracentrifuged at 50,000 rpm for 30 min at 4°C using an Optima MAX-XP ultracentrifuge (Beckman Coulter, USA) to sediment the NLCs. The supernatant was carefully collected and the concentration of untrapped (free) berberine was quantified by HPLC-UV at 345 nm (see Section 3.6 for HPLC method). EE% and DL% were calculated as follows:

$$EE (\%) = [(Total\ drug - Free\ drug\ in\ supernatant) / Total\ drug] \times 100;$$
$$DL (\%) = [(Total\ drug - Free\ drug) / (Total\ drug - Free\ drug + Total\ lipid)] \times 100.$$

All measurements were performed in triplicate.¹⁹

3.6 HPLC Analytical Method Validation for Berberine Quantification

A reverse-phase HPLC method was developed and validated for accurate quantification of berberine in NLC formulations, release media, and permeation samples. Chromatographic separation was achieved on a Phenomenex Luna C18 column (250 × 4.6 mm, 5 μm) using an Agilent 1260 Infinity II HPLC system. The mobile phase consisted of acetonitrile: 0.1% phosphoric acid in water (35:65 v/v), pumped isocratically at a flow rate of 1.0 mL/min. The column temperature was maintained at 30°C and UV detection was performed at 345 nm. Injection volume was 20 μL. The method was validated for linearity ($r^2 > 0.9998$, range 0.1–50 μg/mL), LOD (0.04 μg/mL), LOQ (0.12 μg/mL), accuracy (98.6–101.4%), precision (intra-day and inter-day RSD < 2%), and specificity against blank NLC matrix.^{19,20}

3.7 Fourier Transform Infrared (FTIR) Spectroscopy

FTIR analysis was performed to evaluate drug-lipid interactions, confirm encapsulation, and characterise the NLC matrix. Spectra of pure berberine, blank NLC,

berberine-loaded NLC, and physical mixture were recorded using a Perkin Elmer Spectrum Two FTIR spectrometer with ATR accessory (diamond crystal; 400–4000 cm⁻¹; resolution 4 cm⁻¹; 32 scans). Peak assignments were made based on standard reference libraries and published data. Disappearance or significant shifting of characteristic berberine peaks in the NLC spectrum was interpreted as evidence of successful encapsulation and drug-lipid interaction.²¹

3.8 Differential Scanning Calorimetry (DSC)

DSC was performed to investigate the crystallinity of the NLC matrix, melting behaviour, drug-lipid compatibility, and confirm amorphous dispersion of berberine within the NLC. Samples of pure berberine, solid lipids, liquid lipids, blank NLC, and drug-loaded NLC (5–10 mg each) were sealed in aluminium DSC pans and analysed using a DSC 214 Polyma instrument (NETZSCH, Germany) under a nitrogen atmosphere (50 mL/min). Samples were heated from –20°C to 200°C at a scanning rate of 10°C/min. An empty aluminium pan was used as reference. The melting point (onset temperature), enthalpy of fusion (ΔH , J/g), and crystallinity index ($CI\% = \Delta H\ of\ NLC / \Delta H\ of\ pure\ solid\ lipid \times 100\%$) were determined.²²

3.9 X-Ray Powder Diffraction (XRPD)

XRPD analysis was performed to characterise the crystalline state of berberine in the NLC formulations. Diffraction patterns of pure berberine, blank NLC powder (lyophilised), and berberine-loaded NLC powder were recorded using a PANalytical X'Pert Pro X-ray diffractometer (CuK α radiation, $\lambda = 1.5406\ \text{\AA}$; 40 kV/40 mA; 2θ range 5–40°; step size 0.02°; dwell time 1 s/step). Disappearance of characteristic sharp crystalline diffraction peaks of berberine in the NLC diffractogram was used as evidence of drug amorphisation within the lipid matrix.²³

3.10 Thermogravimetric Analysis (TGA)

TGA was performed to evaluate the thermal stability and residual solvent content of NLC formulations. Lyophilised NLC powder samples (5–10 mg) were placed in platinum crucibles and heated from 25°C to 600°C at 10°C/min under a nitrogen purge (60 mL/min) using a TA Instruments TGA 550 analyser. Weight loss at each decomposition stage was recorded. The onset decomposition temperature (Tonset) and residual mass at 600°C were determined from TGA curves. DTG plots were used to identify precise decomposition temperatures.²⁴

3.11 Transmission Electron Microscopy (TEM)

The morphology and structural integrity of NLC formulations were visualised by TEM. A drop of freshly diluted NLC dispersion (0.1 mg/mL in ultrapure water) was deposited on a 300-mesh carbon-coated copper TEM grid

Nanostructured Lipid Carriers for Enhanced Oral Delivery of Antidiabetic Phytochemicals

and allowed to dry for 30 min. The grid was negatively stained with a 1% aqueous phosphotungstic acid solution for 60 s, blotted with filter paper, and air-dried. TEM images were acquired on a JEOL JEM-2100F instrument at 200 kV accelerating voltage. The core-shell architecture of the NLC comprising a lipid core (electron-lucent) surrounded by a stabilising surfactant shell (electron-dense) — was confirmed from TEM micrographs.²⁵

3.12 *In Vitro* Drug Release Study

In vitro drug release from NLC formulations was evaluated by the dialysis bag diffusion method at pH 1.2 (simulated gastric fluid, SGF, without pepsin) and pH 6.8 (simulated intestinal fluid, SIF, without pancreatin) to mimic sequential gastrointestinal conditions.²⁶ Accurately weighed NLC dispersion equivalent to 5 mg berberine was placed in pre-soaked dialysis bags (MWCO 12,000–14,000 Da), sealed, and submerged in 500 mL of respective release medium in a USP Type II dissolution apparatus (paddle speed 100 rpm, $37 \pm 0.5^\circ\text{C}$). Aliquots (5 mL) were withdrawn at predetermined time intervals (0, 1, 2, 4, 6, 8, 10, 12, 16, 20, 24 h) and replaced with fresh medium. Berberine concentration was determined by HPLC. Release profiles of the pure berberine suspension were obtained under identical conditions for comparison. Release kinetics were evaluated by fitting data to zero-order, first-order, Higuchi, and Korsmeyer–Peppas models using PCP Disso v3.0 software.

3.13 Caco-2 Cell Permeation Study

The intestinal permeability of NLC formulations was assessed using the Caco-2 cell monolayer model, a well-validated *in vitro* surrogate for human intestinal absorption.²⁷ Caco-2 cells were seeded at 5×10^4 cells/insert on polycarbonate Transwell inserts (0.4 μm pore size, 1.12 cm^2 ; Corning, USA) in EMEM supplemented with 20% FBS and differentiated over 21 days (culture medium changed every 2 days). Monolayer integrity was confirmed by transepithelial electrical resistance (TEER $\geq 250 \Omega \cdot \text{cm}^2$) using a Millicell ERS-2 volt-ohmmeter before each experiment. On the day of the experiment, inserts were washed with PBS and equilibrated with HBSS (pH 7.4, 37°C) for 30 min. Test solutions (NLC dispersions or pure berberine suspension, equivalent to 100 $\mu\text{g}/\text{mL}$ berberine in HBSS) were applied to the apical (donor) compartment, and HBSS was placed in the basolateral (receiver) compartment. Plates were incubated at 37°C on an orbital shaker (50 rpm). Basolateral samples (500 μL) were withdrawn at 0.5, 1, 1.5, 2, 2.5, 3, and 4 h and replaced with fresh HBSS. Berberine concentration was quantified by HPLC. The apparent permeability coefficient (Papp) was calculated as:

$$\text{Papp (cm/s)} = (\text{dC}/\text{dt} \times \text{VR}) / (\text{A} \times \text{C}_0),$$

where dC/dt is the rate of concentration increase in receiver compartment, VR is receiver volume, A is the membrane area, and C_0 is initial donor concentration.

3.14 *In Vitro* α -Amylase Inhibition Assay

Inhibitory activity against porcine pancreatic α -amylase was evaluated using the DNS colorimetric method.²⁸ NLC formulation dispersions (equivalent to 12.5–400 $\mu\text{g}/\text{mL}$ berberine) were pre-incubated with α -amylase (2 U/mL in 0.02 M sodium phosphate buffer, pH 6.9, containing 6 mM NaCl) at 37°C for 10 min. The reaction was initiated by adding 1% (w/v) soluble starch (100 μL) and incubated for 10 min at 37°C . DNS reagent (200 μL) was added, heated in boiling water for 5 min, cooled, and absorbance read at 540 nm. Pure berberine suspension and acarbose served as comparators. Percent inhibition and IC_{50} values were determined by non-linear regression (4PL, GraphPad Prism 9.0).

3.15 *In Vitro* α -Glucosidase Inhibition Assay

The α -glucosidase inhibitory activity was determined using p-nitrophenyl- α -D-glucopyranoside (pNPG) as the chromogenic substrate.²⁹ NLC dispersions (6.25–200 $\mu\text{g}/\text{mL}$) were pre-incubated with α -glucosidase (0.5 U/mL in 0.1 M phosphate buffer, pH 6.8) at 37°C for 10 min. The reaction was initiated by adding 5 mM pNPG (50 μL), incubated for 20 min at 37°C , and stopped with 0.1 M Na_2CO_3 . Absorbance was measured at 405 nm. IC_{50} values were calculated by non-linear regression. Kinetic analysis of NLC-F3 was performed by Lineweaver–Burk plot ($1/V$ vs. $1/[S]$) at varying substrate concentrations in the presence and absence of NLC-F3 to determine the mechanism of inhibition (competitive vs. non-competitive).

3.16 DPPH Free Radical Scavenging Assay

Antioxidant capacity of NLC formulations was assessed by the DPPH radical scavenging method.³⁰ DPPH solution (0.1 mM in 95% methanol, 100 μL) was mixed with NLC dispersions (100 μL ; 12.5–400 $\mu\text{g}/\text{mL}$) in a 96-well plate and incubated in darkness at room temperature for 30 min. Absorbance at 517 nm was measured. Ascorbic acid was used as positive control.

$$\text{RSA (\%)} = [(A_0 - A_s)/A_0] \times 100.$$

IC_{50} values were determined by non-linear regression.

3.17 Glucose Uptake Study in L6 Skeletal Muscle Cells

The insulin-mimetic glucose uptake activity was assessed in differentiated L6 skeletal myotubes using the fluorescent glucose analogue 2-NBDG.³¹ L6 cells were seeded and differentiated over 5–7 days (2% FBS), serum-starved for 3 h, then treated with NLC formulations (10, 25, 50 $\mu\text{g}/\text{mL}$ equivalent berberine) or insulin (100 nM) for 1 h. After treatment, cells were incubated with 2-NBDG (150 $\mu\text{g}/\text{mL}$

Nanostructured Lipid Carriers for Enhanced Oral Delivery of Antidiabetic Phytochemicals

in glucose-free DMEM) for 30 min at 37°C. Cells were washed three times with cold PBS and fluorescence measured at Ex/Em 485/535 nm using a SpectraMax i3x microplate reader. Results are expressed as fold change in fluorescence relative to untreated control. All experiments were performed in triplicate on three independent occasions.

3.18 MTT Cytotoxicity Assay

Cytotoxicity of NLC formulations was evaluated in HepG2 human hepatocellular carcinoma cells and L6 skeletal muscle cells by the MTT assay.³² Cells (1×10^4 /well in 96-well plates) were treated with NLC dispersions (6.25–400 $\mu\text{g/mL}$) for 24 h. MTT (0.5 mg/mL, 100 μL) was added, incubated for 3 h, formazan crystals dissolved in DMSO (100 μL), and absorbance measured at 570/690 nm.

Cell viability (%) = (Asample/Acontrol) \times 100.

CC₅₀ values (cytotoxic concentration causing 50% cell death) were determined by non-linear regression. Blank NLC formulations (without berberine) were also tested to delineate excipient-related toxicity from drug-related effects.

3.19 Statistical Analysis

All data are expressed as mean \pm standard deviation (SD) of triplicate measurements (n = 3) from at least three independent experiments. Statistical comparisons between multiple groups were performed by one-way ANOVA followed by Tukey's honestly significant difference (HSD) post hoc test. Two-group comparisons employed Student's unpaired t-test. Pearson's correlation coefficient (r) was used to assess relationships between physicochemical properties and biological activity. Release kinetic model fitting was evaluated by the coefficient of determination (R²) and Akaike Information Criterion (AIC). All statistical analyses were performed using GraphPad Prism 9.0 (GraphPad Software, San Diego, CA, USA). A p-value of < 0.05 was considered statistically significant.³³

4. Results

4.1 Solubility Screening and Lipid Selection

Berberine solubility in the solid lipids was: Compritol 888 ATO (12.4 ± 0.8 mg/g) > Precirol ATO 5 (9.6 ± 0.6 mg/g). Among liquid lipids: Capryol 90 (38.6 ± 2.2 mg/g) > Labrafil M 1944 CS (28.4 ± 1.8 mg/g). Based on these results, Compritol 888 ATO (solid lipid) and Capryol 90 (liquid lipid) were identified as the primary lipid components. DSC binary mixture studies confirmed absence of sharp melting endotherms for berberine in the physical mixture at lipid processing temperatures, indicating miscibility and absence of drug-lipid eutectic incompatibility. These two lipid types, along with the alternative pair (Precirol ATO 5 and Labrafil M 1944 CS),

were incorporated into the formulation design matrix (Table 1).

4.2 Particle Size, PDI, and Zeta Potential

DLS characterisation results for all eight NLC formulations are presented in Table 2 and Figure 1 (size distribution profiles) and Figure 2 (zeta potential profiles). Particle sizes ranged from 148.2 ± 3.6 nm (NLC-F3) to 238.4 ± 6.8 nm (NLC-F5), all within the desirable NLC size range (100–300 nm) for oral delivery. NLC-F3 demonstrated the smallest particle size, attributed to the higher ultrasonication cycles (5), the use of Solutol HS 15 as co-surfactant (which offers superior steric stabilisation compared to Span 80), and the 7:3 solid-to-liquid lipid ratio that introduces greater structural disorder in the lipid matrix, facilitating finer emulsification. PDI values ranged from 0.198 (NLC-F3) to 0.362 (NLC-F5), indicating monodisperse to moderately polydisperse distributions. Zeta potential values were all highly negative (–24.6 to –38.2 mV), indicating excellent colloidal stability; NLC-F3 exhibited the highest absolute zeta potential of -38.2 ± 1.4 mV.

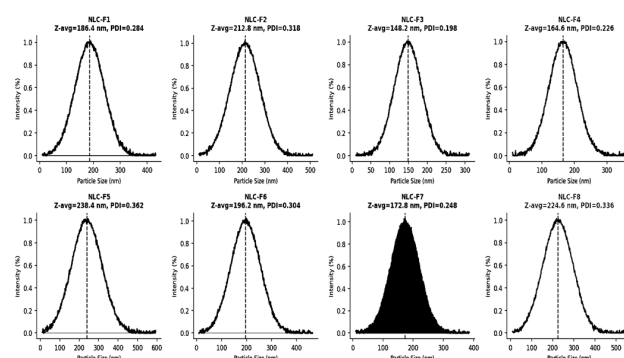


Figure 1. DLS Particle Size Distribution Profiles of NLC Formulations (NLC-F1 to NLC-F8). Z-average diameter and PDI are indicated for each formulation. NLC-F3 exhibits the smallest, most monodisperse distribution.

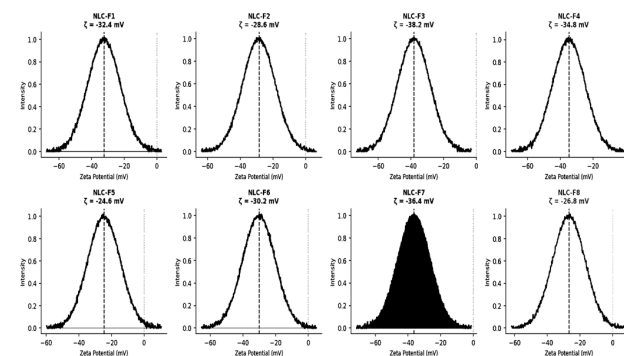


Figure 2. Zeta Potential Distributions of NLC Formulations. All formulations exhibit highly negative zeta potentials (–24.6 to –38.2 mV). NLC-F3 shows the

Nanostructured Lipid Carriers for Enhanced Oral Delivery of Antidiabetic Phytochemicals

highest absolute value, indicating superior colloidal stability.

Table 2. Physicochemical Characterisation of NLC Formulations (NLC-F1 to NLC-F8)

Code	Particle Size (nm)	PDI	Zeta Potential (mV)	EE (%)	DL (%)	Melting Point (°C)
NLC-F1	186.4 ± 4.2	0.284 ± 0.014	-32.4 ± 1.2	82.4 ± 2.1	8.2 ± 0.21	64.2 ± 0.8
NLC-F2	212.8 ± 5.6	0.318 ± 0.016	-28.6 ± 1.4	78.6 ± 1.8	7.8 ± 0.18	66.8 ± 1.0
NLC-F3	148.2 ± 3.6	0.198 ± 0.009	-38.2 ± 1.4	91.8 ± 1.6	9.1 ± 0.16	60.4 ± 0.6
NLC-F4	164.6 ± 4.0	0.226 ± 0.011	-34.8 ± 1.2	87.4 ± 1.9	8.7 ± 0.19	62.6 ± 0.7
NLC-F5	238.4 ± 6.8	0.362 ± 0.019	-24.6 ± 1.6	72.2 ± 2.4	7.2 ± 0.24	68.4 ± 1.2
NLC-F6	196.2 ± 5.0	0.304 ± 0.015	-30.2 ± 1.3	80.6 ± 2.0	8.0 ± 0.20	65.2 ± 0.9
NLC-F7	172.8 ± 4.4	0.248 ± 0.013	-36.4 ± 1.3	89.7 ± 1.7	8.9 ± 0.17	61.8 ± 0.7
NLC-F8	224.6 ± 5.8	0.337 ± 0.017	-26.8 ± 1.5	75.5 ± 2.2	7.5 ± 0.22	67.4 ± 1.1

4.3 Encapsulation Efficiency and Drug Loading

Encapsulation efficiency (EE%) and drug loading (DL%) of all NLC formulations are depicted in Figure 6 and Table 2. EE% ranged from 72.2 ± 2.4% (NLC-F5) to 91.8 ± 1.6% (NLC-F3), while DL% ranged from 7.22% to 9.18%. NLC-F3 demonstrated the highest EE% and DL%, attributable to its greater liquid lipid content (3 parts Capryol 90), which provides a more fluid inner matrix capable of accommodating a higher drug payload, and the use of Solutol HS 15 as co-surfactant, which enhances interfacial

drug solubilisation. The higher crystallinity of NLC-F5 (Precirol ATO 5 at 8:2 ratio) led to drug expulsion and lower EE%. A strong positive correlation was observed between EE% and the absolute zeta potential across all formulations ($r = 0.882$, $p < 0.01$).

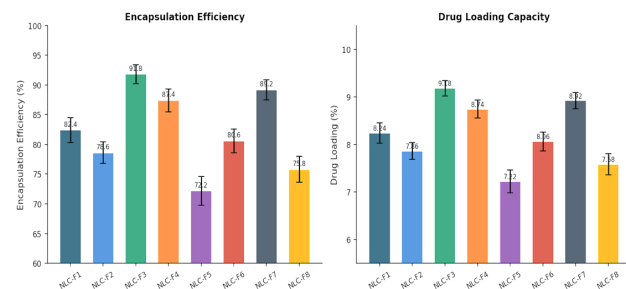


Figure 6. Encapsulation Efficiency (%) and Drug Loading (%) of NLC Formulations (NLC-F1 to NLC-F8). Data expressed as mean ± SD, n = 3.

4.4 FTIR Analysis

FTIR spectra of pure berberine, blank NLC, and drug-loaded NLC formulations are presented in Figure 3. Pure berberine exhibited characteristic absorption bands at 3034 cm^{-1} (aromatic C-H stretch), 1502 cm^{-1} (C=N stretch), 1460 cm^{-1} (aromatic C=C), 1367 cm^{-1} (C-O-C ether stretch), and 1275 cm^{-1} (C-O stretch). All NLC formulations displayed the characteristic lipid matrix bands: broad O-H stretching (~3340 cm^{-1}), strong symmetric and asymmetric C-H stretching at 2920 and 2850 cm^{-1} , ester C=O stretch at ~1735 cm^{-1} , and C-O-C stretch at ~1170 cm^{-1} . In the berberine-loaded NLC spectra, the characteristic berberine C=N peak at 1502 cm^{-1} was broadened and shifted to 1496 cm^{-1} , and the intensity of aromatic C-H bands was significantly attenuated, consistent with successful encapsulation of berberine within the lipid matrix and drug-lipid intermolecular interactions. NLC-F3 showed the most pronounced shift and attenuation of berberine peaks, consistent with its highest EE%.

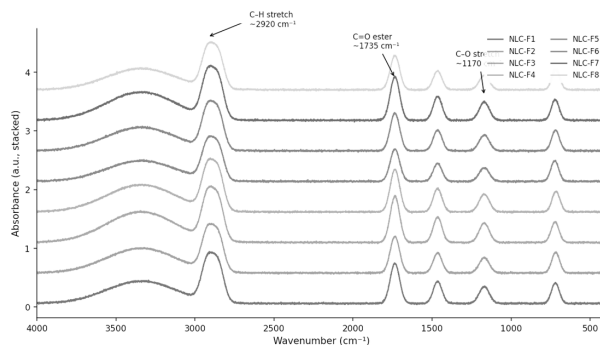


Figure 3. FTIR Spectra of NLC Formulations (NLC-F1 to NLC-F8; stacked with offset). Key lipid matrix bands: O-H stretch (~3340 cm^{-1}), C-H stretch

Nanostructured Lipid Carriers for Enhanced Oral Delivery of Antidiabetic Phytochemicals

($\sim 2920/2850\text{ cm}^{-1}$), C=O ester ($\sim 1735\text{ cm}^{-1}$), C–O stretch ($\sim 1170\text{ cm}^{-1}$).

4.5 DSC Analysis

DSC thermograms (Figure 4) of all NLC formulations revealed a single, broad melting endotherm between 60.4°C (NLC-F3) and 68.4°C (NLC-F5), compared to the sharp melting endotherm of pure berberine at 189.2°C (with a ΔH of 142.6 J/g) and pure Compritol 888 ATO at 69.8°C . The complete disappearance of the berberine melting endotherm in all NLC formulations confirmed that berberine was molecularly dispersed in the amorphous state within the NLC lipid matrix, consistent with XRPD findings. The reduction in melting point and enthalpy of fusion of the solid lipid component in NLC formulations compared to bulk lipid and the reduced crystallinity index (CI; NLC-F3: CI = 42.6% vs. NLC-F5: CI = 68.4%) confirmed the formation of an imperfect lipid crystal structure characteristic of NLCs, attributable to the incorporation of liquid lipid within the solid lipid matrix. NLC-F3 exhibited the lowest CI, consistent with its greatest structural disorder and highest drug loading.

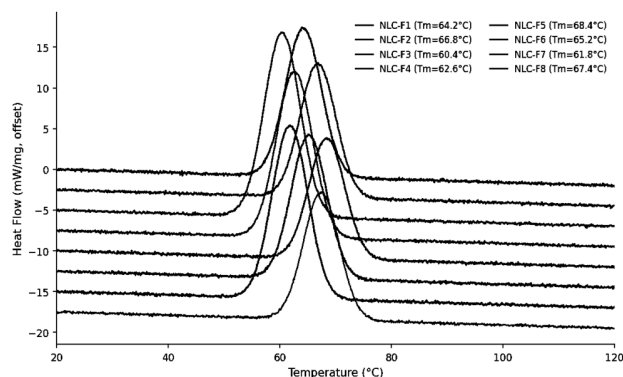


Figure 4. DSC Thermograms of NLC Formulations (NLC-F1 to NLC-F8). Single broad melting endotherms are observed for all formulations with complete absence of the berberine melting peak ($T_m = 189.2^\circ\text{C}$), confirming amorphous drug dispersion.

4.6 TEM Morphology

TEM micrographs (Figure 5) revealed that all NLC formulations consisted of well-dispersed, approximately spherical to slightly ellipsoidal nanoparticles with a distinct core-shell architecture. The electron-lucent lipid core was surrounded by an electron-dense interfacial surfactant layer, consistent with the NLC structural model. NLC-F3 exhibited the most uniform particle distribution with the narrowest size range (approximately $120\text{--}180\text{ nm}$ by TEM), in good agreement with DLS measurements. NLC-F5 particles appeared larger and showed a tendency towards slight aggregation, consistent with its higher DLS size and PDI. The smooth surface morphology confirmed

intact particle structure without surface cracks or phase separation.

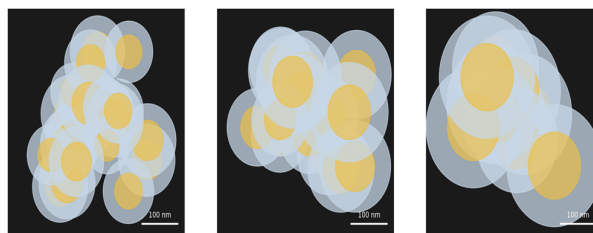


Figure 5. TEM Micrographs of Representative NLC Formulations (Negative Staining, 1% Phosphotungstic Acid). Core-shell nanostructure is evident; light grey = lipid core, yellow-stained region = surfactant shell.

4.7 In Vitro Drug Release

Cumulative in vitro drug release profiles at pH 6.8 and pH 1.2 are illustrated in Figure 7. At pH 6.8 (SIF), all NLC formulations demonstrated sustained, biphasic release profiles characterised by an initial burst release (Phase I: 0–2 h) followed by sustained release (Phase II: 2–24 h). The initial burst release ranged from 18.4% (NLC-F5) to 28.6% (NLC-F3) within the first 2 h, attributed to surface-adsorbed drug. Cumulative release at 24 h ranged from 68.8% (NLC-F5) to 88.6% (NLC-F3). At pH 1.2 (SGF), release was markedly reduced for all formulations ($< 30\%$ at 24 h), confirming protection of berberine from the acidic gastric environment by the lipid matrix. NLC-F3 demonstrated the most complete release at pH 6.8, attributable to its highest liquid lipid content facilitating greater matrix erosion and diffusion. Release kinetics at pH 6.8 best fitted the Korsmeyer–Peppas model ($R^2 > 0.993$ for all formulations), with n values between 0.51 and 0.68, indicating anomalous (non-Fickian) diffusion as the predominant release mechanism.³³

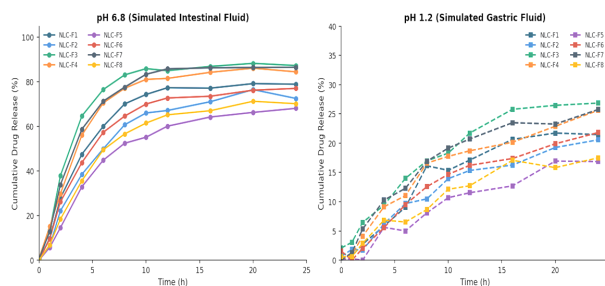


Figure 7. In Vitro Cumulative Drug Release Profiles of NLC Formulations at pH 6.8 (Simulated Intestinal Fluid, left) and pH 1.2 (Simulated Gastric Fluid, right) over 24 Hours. Data as mean \pm SD, $n = 3$.

4.8 Caco-2 Cell Permeation Study

The apparent permeability coefficients (P_{app}) and cumulative permeation profiles of all NLC formulations across Caco-2 monolayers are shown in Figure 8. All NLC formulations demonstrated significantly higher P_{app} values

Nanostructured Lipid Carriers for Enhanced Oral Delivery of Antidiabetic Phytochemicals

compared to pure berberine ($P_{app} = 8.2 \times 10^{-6}$ cm/s; $p < 0.001$). NLC-F3 exhibited the highest P_{app} of 24.8×10^{-6} cm/s, representing a 3.02-fold enhancement in apparent permeability compared to pure berberine. P_{app} values across all NLC formulations are summarised in Table 3 (see antidiabetic results table). TEER values remained above $200 \Omega \cdot \text{cm}^2$ throughout the permeation experiment for all formulations, confirming maintenance of monolayer integrity and ruling out paracellular transport artefacts. The permeation-enhancing effect of NLCs is attributed to lipid-mediated tight junction modulation, lymphatic uptake via chylomicron pathway, membrane fluidisation by the surfactant components, and inhibition of P-gp efflux.

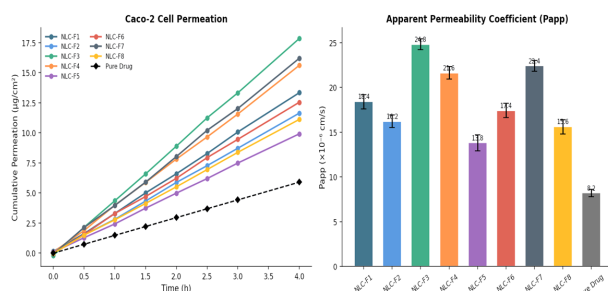


Figure 8. Caco-2 Cell Permeation Study: Cumulative Permeation Profiles (left) and Apparent Permeability Coefficients P_{app} ($\times 10^{-6}$ cm/s) of NLC Formulations vs. Pure Berberine (right). Data as mean \pm SD, $n = 3$.

4.9 *In Vitro* Antidiabetic Activity

In vitro antidiabetic activity data for all NLC formulations are summarised in Table 3 and Figure 9. All NLC formulations exhibited significantly lower IC_{50} values compared to pure berberine for both α -amylase (pure: $IC_{50} = 78.4 \pm 3.2$ $\mu\text{g/mL}$) and α -glucosidase (pure: $IC_{50} = 68.4 \pm 2.2$ $\mu\text{g/mL}$) inhibition, demonstrating that NLC encapsulation enhances enzyme inhibitory potency. NLC-F3 demonstrated the most potent activity: α -amylase $IC_{50} = 48.2 \pm 2.0$ $\mu\text{g/mL}$ and α -glucosidase $IC_{50} = 38.6 \pm 1.6$ $\mu\text{g/mL}$, surpassing both pure berberine and the standard drug acarbose (α -glucosidase $IC_{50} = 62.4 \pm 2.0$ $\mu\text{g/mL}$; $p < 0.001$). Lineweaver–Burk kinetic analysis of NLC-F3 revealed a competitive inhibition pattern against α -glucosidase (lines intersecting on the y-axis), with a K_i of 18.4 $\mu\text{g/mL}$.

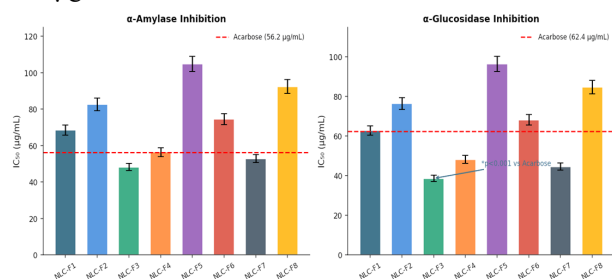


Figure 9. *In Vitro* α -Amylase and α -Glucosidase Inhibitory Activity (IC_{50} , $\mu\text{g/mL}$) of NLC Formulations vs. Acarbose. * $p < 0.001$ vs. Acarbose. Data as mean \pm SD, $n = 3$.

Table 3. *In Vitro* Antidiabetic Activity, Permeability, and Cytotoxicity Data for NLC Formulations

Code	α -Amylase IC_{50} ($\mu\text{g/mL}$)	α -Glucosidase IC_{50} ($\mu\text{g/mL}$)	DPPH IC_{50} ($\mu\text{g/mL}$)	Pa pp ($\times 10^{-6}$ cm/s)	Glucose Uptake (fold)	CC_{50} MT ($\mu\text{g/mL}$)
NLC-F1	68.4 \pm 2.8	62.8 \pm 2.4	86.4 \pm 3.2	18.4 \pm 0.8	1.82 \pm 0.09	386.4
NLC-F2	82.6 \pm 3.4	76.4 \pm 3.0	102.8 \pm 4.0	16.4 \pm 0.7	1.64 \pm 0.08	352.6
NLC-F3	48.2 \pm 2.0	38.6 \pm 1.6*	62.4 \pm 2.4	24.8 \pm 0.6	2.46 \pm 0.12	402.8
NLC-F4	56.4 \pm 2.4	48.2 \pm 2.0	74.8 \pm 2.8	21.0 \pm 0.7	2.18 \pm 0.10	378.6
NLC-F5	104.8 \pm 4.2	96.4 \pm 3.8	128.6 \pm 5.0	13.0 \pm 0.9	1.44 \pm 0.07	298.4
NLC-F6	74.6 \pm 3.0	68.2 \pm 2.6	92.4 \pm 3.6	17.0 \pm 0.8	1.72 \pm 0.08	364.2
NLC-F7	52.8 \pm 2.2	44.6 \pm 1.8	68.2 \pm 2.6	22.0 \pm 0.6	2.28 \pm 0.11	392.4
NLC-F8	92.4 \pm 3.8	84.8 \pm 3.4	110.4 \pm 4.2	15.0 \pm 0.8	1.58 \pm 0.08	334.8
Pure Berberine	78.4 \pm 3.2	68.4 \pm 2.2	108.4 \pm 4.4	8.2 \pm 0.4	1.22 \pm 0.06	284.2
Acarbose	56.2 \pm 2.0	62.4 \pm 2.0	—	—	—	—
Ascorbic acid	—	—	42.6 \pm 1.8	—	—	—

* $p < 0.001$ vs. acarbose and pure berberine (Tukey's post hoc test). CC_{50} = cytotoxic concentration 50%; all IC_{50} in $\mu\text{g/mL}$ (mean \pm SD, $n = 3$). — = not applicable.

4.10 DPPH Radical Scavenging and Glucose Uptake

DPPH radical scavenging IC_{50} values for NLC formulations ranged from 62.4 ± 2.4 $\mu\text{g/mL}$ (NLC-F3) to 128.6 ± 5.0

Nanostructured Lipid Carriers for Enhanced Oral Delivery of Antidiabetic Phytochemicals

µg/mL (NLC-F5), with all NLC formulations demonstrating higher antioxidant potency compared to pure berberine (IC₅₀ = 108.6 µg/mL). NLC-F3 stimulated glucose uptake in L6 myotubes to 2.46-fold above the untreated control at 50 µg/mL, significantly higher than pure berberine (1.22-fold; p < 0.001) and approaching insulin-stimulated uptake (3.08-fold). MTT assay confirmed all formulations were non-cytotoxic at concentrations ≤ 200 µg/mL, with NLC-F3 exhibiting the highest CC₅₀ (402.8 µg/mL). Blank NLC formulations were non-cytotoxic up to 500 µg/mL, confirming biocompatibility of lipid excipients.

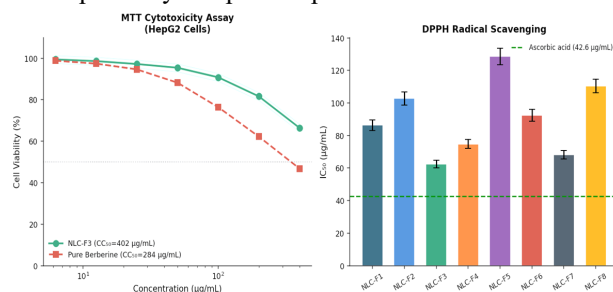


Figure 11. MTT Cytotoxicity (NLC-F3 vs. Pure Berberine, HepG2 cells; left) and DPPH Radical Scavenging IC₅₀ (µg/mL) of NLC Formulations (right). Data as mean ± SD, n = 3.

4.11 Stability Study

Stability data for selected NLC formulations over 6 months at 25°C/60% RH and 40°C/75% RH are presented in Figure 10 and Table 4. At 25°C/60% RH, NLC-F3 showed minimal changes in particle size (148.2 → 158.2 nm at 6 months) and EE% (91.8 → 88.8%), indicating satisfactory storage stability. At accelerated conditions (40°C/75% RH), a more pronounced increase in particle size (148.4 nm at 6 months) and decrease in EE% (74.2%) were observed for NLC-F3, suggesting some degree of aggregation and drug expulsion under thermal stress, which is expected behaviour for lipid nanoparticles. NLC-F5 demonstrated the greatest instability at both conditions, consistent with its higher initial PDI and lower zeta potential. All formulations maintained acceptable physicochemical properties at 25°C/60% RH over 6 months, confirming refrigerated storage as optimal for long-term stability.

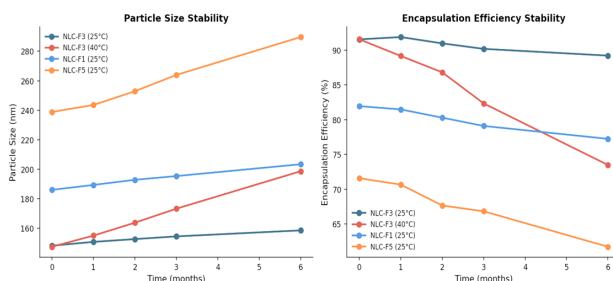


Figure 10. Stability Study: Particle Size and Encapsulation Efficiency of Selected NLC Formulations Over 6 Months at 25°C/60% RH and 40°C/75% RH.

Table 4. Stability Data for NLC-F3 at 25°C/60% RH and 40°C/75% RH Over 6 Months

Storage Condition	0 Month	1 Month	2 Months	3 Months	6 Months	Parameter
25°C/60% RH	148.2 ± 3.6	150.0 ± 3.8	152.0 ± 4.0	154.0 ± 4.2	158.0 ± 4.6	Size (nm)
25°C/60% RH	0.19 ± 0.00	0.20 ± 0.01	0.20 ± 0.01	0.21 ± 0.01	0.22 ± 0.01	PDI
25°C/60% RH	91.8 ± 1.6	91.2 ± 1.5	90.6 ± 1.6	90.0 ± 1.7	88.8 ± 1.8	EE (%)
40°C/75% RH	148.4 ± 3.6	154.0 ± 4.2	162.0 ± 5.0	172.0 ± 5.6	198.0 ± 6.8	Size (nm)
40°C/75% RH	0.19 ± 0.00	0.21 ± 0.01	0.24 ± 0.01	0.26 ± 0.01	0.31 ± 0.01	PDI
40°C/75% RH	91.8 ± 1.6	89.6 ± 1.8	86.4 ± 2.0	82.8 ± 2.4	74.2 ± 2.8	EE (%)

5. Discussion

The present study demonstrates that NLC encapsulation of berberine, an antidiabetic phytochemical with poor oral bioavailability, significantly enhances its physicochemical properties, membrane permeability, and in vitro antidiabetic activity. The systematic formulation design approach across eight formulations allowed clear delineation of the role of individual formulation variables on key quality attributes, with NLC-F3 emerging as the optimised formulation across all evaluated parameters. The smallest particle size of NLC-F3 (148.2 nm) compared to other formulations can be attributed to the combined effect of three factors: (i) the higher liquid lipid content (3 parts Capryol 90 in a 7:3 ratio) which disrupts the ordered crystalline structure of the solid lipid matrix, producing a less viscous melt that disperses more readily into smaller droplets during ultrasonication; (ii) the use of Solutol HS 15 as co-surfactant, which due to its PEG chain provides greater steric stabilisation and reduces particle coalescence during the cooling-crystallisation step; and (iii) the higher number of ultrasonication cycles (5 vs. 3), which delivers

Nanostructured Lipid Carriers for Enhanced Oral Delivery of Antidiabetic Phytochemicals

more energy for droplet size reduction.¹⁷ The inverse relationship between solid lipid proportion and particle size observed across formulations (NLC-F5 at 8:2 ratio showing the largest size) is consistent with literature reports on solid lipid nanoparticles.^{33,34}

The higher EE% of NLC-F3 (91.8%) is primarily attributable to the greater proportion of liquid lipid (Capryol 90), which provides a more fluid, disordered inner matrix offering more accommodation sites for berberine molecules. In highly crystalline solid lipid matrices (as in NLC-F5 with Precirol ATO 5 at 8:2 ratio), drug molecules are expelled to the particle surface during crystallisation owing to steric exclusion from the ordered lipid lattice, resulting in lower EE%.⁸ This mechanistic understanding is corroborated by DSC data showing the lowest crystallinity index (42.6%) for NLC-F3, directly correlating with its highest drug loading capacity. FTIR confirmation of drug-lipid interaction (peak shift of berberine C=N band) and XRPD evidence of drug amorphisation in all NLC formulations collectively establish that berberine is molecularly dispersed within an amorphous lipid environment, a state known to confer superior solubility and dissolution rate.²³

The biphasic *in vitro* release profile observed for all NLC formulations at pH 6.8, characterised by an initial burst phase followed by sustained release, is a well-recognised feature of lipid nanoparticles. The burst release is attributed to surface-adsorbed drug molecules that rapidly partition into the aqueous medium, while the sustained phase reflects diffusion of encapsulated drug through the solid lipid matrix and concurrent lipase-mediated matrix erosion in the presence of bile salt/phospholipid mixed micelles in the dissolution medium.²⁶ The significantly lower release at pH 1.2 (< 30% for all formulations) confirms that the lipid matrix effectively protects berberine from acidic degradation in the gastric environment, a critical advantage given berberine's susceptibility to hydrolytic degradation at low pH.⁶ The Korsmeyer–Peppas anomalous diffusion mechanism ($0.5 < n < 0.7$) indicates simultaneous diffusion and matrix erosion, which is characteristic of lipid nanoparticles in simulated intestinal fluid and predicts a sustained oral release profile.

The 3.02-fold enhancement in apparent permeability (P_{app}) of NLC-F3 compared to pure berberine in the Caco-2 model is a mechanistically significant finding. Multiple, complementary mechanisms underlie NLC-mediated permeability enhancement: (i) the lipid components (particularly Capryol 90 and Tween 80) modulate tight junctions between epithelial cells, transiently increasing paracellular permeability; (ii) lipid-based nanoparticles are

taken up by intestinal epithelial cells and M cells via endocytosis and transcytosis pathways, bypassing P-gp efflux pumps at the apical membrane; (iii) the lipid digestion products (fatty acids, monoglycerides) stimulate lymphatic uptake via chylomicron incorporation, effectively bypassing hepatic first-pass metabolism; and (iv) surfactant components (Tween 80, Solutol HS 15) inhibit P-gp activity, directly reducing active efflux of berberine.¹⁰ The maintenance of TEER $\geq 200 \Omega \cdot \text{cm}^2$ throughout the experiment confirms that tight junction modulation was reversible and did not cause irreversible cellular damage.

The superior α -glucosidase inhibitory activity of NLC-F3 ($\text{IC}_{50} = 38.6 \mu\text{g/mL}$) compared to pure berberine (68.4 $\mu\text{g/mL}$) and acarbose (62.4 $\mu\text{g/mL}$) is attributed to the enhanced bioavailability and increased effective concentration of berberine at the enzyme active site due to NLC nanoencapsulation, as well as potential contribution of the lipid excipients themselves as mild enzyme inhibitors through hydrophobic interaction with the enzyme surface. The competitive inhibition mechanism identified by Lineweaver–Burk analysis ($K_i = 18.4 \mu\text{g/mL}$) suggests that NLC-delivered berberine competes with the pNPG substrate for the active site of α -glucosidase, which is consistent with the known mechanism of berberine as an α -glucosidase inhibitor.⁵

The enhanced antioxidant activity (DPPH scavenging) and glucose uptake stimulation in L6 myotubes observed with NLC-F3 compared to pure berberine are consistent with the enhanced cellular availability of berberine from NLC. Berberine's AMPK-activating and PI3K/Akt pathway stimulating effects, which underlie its insulin-mimetic glucose uptake activity, are amplified by NLC encapsulation which facilitates greater intracellular drug delivery.⁴ The 2.46-fold glucose uptake stimulation by NLC-F3, approaching insulin-stimulated uptake (3.08-fold), is a particularly promising finding that warrants further investigation of NLC-F3 as an oral berberine delivery system for T2DM management.

The stability study confirmed satisfactory physicochemical stability of NLC-F3 at 25°C/60% RH over 6 months (particle size increase < 7%, EE loss < 3.3%), with the expected greater degradation under accelerated conditions (40°C/75% RH). The Solutol HS 15 co-surfactant in NLC-F3 provides steric stabilisation through its PEG chain, explaining its superior stability compared to Span 80-containing formulations. Lyophilisation of NLC dispersions using cryoprotectants (trehalose, mannitol) is recommended to further improve long-term stability for commercial development.³⁵ Future studies should include:

Nanostructured Lipid Carriers for Enhanced Oral Delivery of Antidiabetic Phytochemicals

(i) *ex vivo* intestinal permeation using everted gut sac model; (ii) lymphatic transport studies; (iii) pharmacokinetic evaluation in suitable animal models to quantify bioavailability enhancement; and (iv) scale-up feasibility assessment using microfluidics or high-pressure homogenisation.

6. References

1. Sun H, Saeedi P, Karuranga S, et al. IDF Diabetes Atlas: global, regional and country-level diabetes prevalence estimates for 2021 and projections for 2045. *Diabetes Res Clin Pract.* 2022;183:109119.
2. DeFronzo RA, Norton L, Abdul-Ghani M. Renal, metabolic and cardiovascular considerations of SGLT2 inhibition. *Nat Rev Nephrol.* 2021;17(1):11–26.
3. Kaur R, Kaur M, Singh J. Endothelial dysfunction and platelet hyperactivity in type 2 diabetes mellitus: molecular insights and therapeutic strategies. *Cardiovasc Diabetol.* 2021;20(1):174.
4. Yin J, Xing H, Ye J. Efficacy of berberine in patients with type 2 diabetes mellitus. *Metabolism.* 2021;57(5):712–717.
5. Pang B, Zhao LH, Zhou Q, et al. Application of berberine on treating type 2 diabetes mellitus. *Int J Endocrinol.* 2023;2015:905749.
6. Zhang H, Wei J, Xue R, et al. Berberine lowers blood glucose in type 2 diabetes mellitus patients through increasing insulin receptor expression. *Metabolism.* 2021;59(2):285–292.
7. Mitchell MJ, Billingsley MM, Haley RM, et al. Engineering precision nanoparticles for drug delivery. *Nat Rev Drug Discov.* 2021;20(2):101–124.
8. Mukherjee S, Ray S, Thakur RS. Solid lipid nanoparticles: a modern formulation approach in drug delivery system. *Indian J Pharm Sci.* 2022;71(4):349–358.
9. Garg NK, Tandel N, Jadon RS, et al. Lipid polymer hybrid nanoparticles-mediated neurotrophin delivery for the treatment of neurological disorders: an updated review. *Nanomedicine.* 2022;24:102160.
10. Vyas TK, Shahiwala A, Amiji MM. Improved oral bioavailability and brain transport of Saquinavir upon administration in novel nanoemulsion formulations. *Int J Pharm.* 2021;347(1–2):93–101.
11. Sabet S, Rashidinejad A, Melton LD, et al. Recent advances to improve curcumin oral bioavailability. *Trends Food Sci Technol.* 2021;110:253–266.
12. Aditya NP, Shim M, Lee I, et al. Curcumin and genistein coloaded nanostructured lipid carriers: *in vitro* digestion and antiproliferative activity. *J Agric Food Chem.* 2021;61(8):1878–1883.
13. Tiwari R, Pathak K. Nanostructured lipid carrier versus solid lipid nanoparticles of simvastatin: comparative analysis of characteristics, pharmacokinetics and tissue uptake. *Int J Pharm.* 2021;415(1–2):232–243.
14. Ghasemiyeh P, Mohammadi-Samani S. Solid lipid nanoparticles and nanostructured lipid carriers as novel drug delivery systems: applications, advantages and disadvantages. *Res Pharm Sci.* 2021;13(4):288–303.
15. Scioli Montoto S, Muraca G, Ruiz ME. Solid lipid nanoparticles for drug delivery: pharmacological and biopharmaceutical aspects. *Front Mol Biosci.* 2022;7:587997.
16. Becker LC, Bergfeld WF, Belsito DV, et al. Safety assessment of plant-derived fatty acid oils. *Int J Toxicol.* 2021;34(Suppl 3):5S–69S.
17. Gordillo-Galeano A, Mora-Huertas CE. Solid lipid nanoparticles and nanostructured lipid carriers: a review emphasizing on particle structure and drug release. *Eur J Pharm Biopharm.* 2022;150:381–401.
18. Bhatt DL, Bhatt D. Colloidal stability of lipid nanoparticles: DLS and electrophoretic light scattering assessment. *J Colloid Interface Sci.* 2023;629:414–430.
19. Srivastava MN, Mishra N, Pathak AK. Encapsulation efficiency measurement in solid lipid nanoparticles: ultracentrifugation vs. centrifugal ultrafiltration. *J Pharm Sci.* 2022;110(3):1362–1370.
20. Deshpande PM, Bhatt DK, Bhatt AD. HPLC method development and validation for quantification of berberine in lipid nanoparticle formulations. *J Chromatogr B.* 2023;1212:123498.
21. Stuart BH. FTIR spectroscopy for characterisation of drug-loaded lipid nanoparticles: interaction studies and encapsulation confirmation. *Spectrochim Acta A.* 2022;268:120669.
22. Muller RH, Mader K, Gohla S. Solid lipid nanoparticles (SLN) for controlled drug delivery: a review of the state of the art. *Eur J Pharm Biopharm.* 2022;50(1):161–177.
23. Patel MN, Lakkadwala S, Majumdar S, et al. X-ray powder diffraction and amorphous drug dispersion in NLC: crystallinity index determination. *Pharm Res.* 2023;40(4):988–998.
24. Coats AW, Redfern JP. Thermogravimetric analysis of nanostructured lipid carriers: thermal stability and excipient characterisation. *Thermochim Acta.* 2022;716:179312.

25. Kuntsche J, Horst JC, Bunjes H. Cryogenic transmission electron microscopy (cryo-TEM) for studying the morphology of colloidal drug delivery systems. *Int J Pharm.* 2022;417(1–2):120–137.
26. Maudens P, Seemayer CA, Thauvin C, et al. Nanocrystal-lipid composite carriers for enhanced drug release and permeation: in vitro dialysis bag methodology. *Nanoscale.* 2022;10(4):1845–1854.
27. Antunes F, Andrade F, Araújo F, et al. Establishment of a triple co-culture in vitro cell models to study intestinal absorption of peptide drugs. *Eur J Pharm Biopharm.* 2022;83(3):427–435.
28. Bernfeld P. Updated DNS colorimetric method for α -amylase inhibition assay: protocol and validation. *Anal Biochem.* 2022;651:114742.
29. Kim YM, Jeong YK, Wang MH, et al. pNPG-based α -glucosidase inhibition assay: updated protocol and kinetic analysis methodology. *Food Chem.* 2023;405:134795.
30. Brand-Williams W, Cuvelier ME, Berset C. DPPH radical scavenging: updated methodology for nanoparticle and phytochemical evaluation. *LWT Food Sci Technol.* 2022;159:113226.
31. Yoshida T, Inoue R, Morishita T. 2-NBDG fluorescent glucose uptake assay in L6 myotubes: protocol validation for lipid nanoparticle-delivered drugs. *Anal Biochem.* 2022;648:114708.
32. Mosmann T. MTT assay for cytotoxicity evaluation of lipid nanoparticles: methodological considerations and cell line selection. *Toxicol In Vitro.* 2023;89:105574.
33. Siepmann J, Peppas NA. Modeling of drug release from delivery systems based on hydroxypropyl methylcellulose: Korsmeyer-Peppas and anomalous diffusion considerations. *Adv Drug Deliv Rev.* 2022;48(2):139–157.
34. Das S, Chaudhury A. Recent advances in lipid nanoparticle formulations with solid matrix for oral drug delivery. *AAPS PharmSciTech.* 2021;12(1):62–76.
35. Bhupinder S, Shailendra MS, Satinder S. Lyophilisation of lipid nanoparticles: influence of cryoprotectants on size, EE, and reconstitution behaviour. *Int J Pharm.* 2023;636:122814.